JOURNAL OF COMPUTATIONAL PHYSICS 104, 110-117 (1993)

Two Modified Staging Algorithms for Path Integral Monte Carlo Simulations

L. CRUZEIRO-HANSSON, J. O. BAUM,* AND J. L. FINNEY*

Department of Crystallography, Birkbeck College, Malet St., London WC1E 7HX, United Kingdom

Received January 18, 1991; revised August 21, 1991

Two algorithms which mix a staging procedure with a conventional Metropolis importance sampling are derived. Their applicability in simulating the thermal equilibrium properties of quantum systems is tested in three systems: a quantum free particle, an electron in a hard spheres crystal, and an electron in helium. We conclude that the two algorithms are generally more efficient than others used previously for the same systems, with a further advantage of being machine independent and able to deal with both hard core and smooth potentials. We also show that it is possible to model the properties of the electron in helium with a hard core potential for the interaction of the electron with helium as well as the helium–helium interaction.

1. INTRODUCTION

Feynman's path integral formulation of quantum statistical mechanics [1] makes possible the computer simulation of the thermal properties of quantum systems. Indeed, the statistical–mechanical properties of a quantum system may be determined from the density matrix $\rho(r_0, r_P; \beta)$

$$\rho(r_0, r_P; \beta) = \langle r_0 | e^{-\beta \hat{H}} | r_P \rangle, \tag{1}$$

where $\beta = 1/kT$, k being Boltzmann's constant, T the absolute temperature, and $\hat{H}$ the Hamiltonian of the system. Applying repeatedly the partition of the unity matrix in terms of a complete set of eigenstates $|r\rangle$ leads to

$$\rho(r_0, r_P; \beta) = \int \cdots \int \prod_{i=1}^{P-1} dr_i \, \rho(r_0, r_1; \tau) \times \rho(r_1, r_2; \tau) \cdots \rho(r_{P-1}, r_P; \tau), \tag{2}$$

where $\tau = \beta/P$. For τ sufficiently small, the high-temperature approximation of the density matrix is valid and

$$\rho(r_i, r_{i+1}; \tau) = \left(\frac{P}{2\pi\lambda^2}\right)^{3/2} \exp\left[-\frac{P}{2\lambda^2}(r_{i+1} - r_i)^2\right] \times \exp\left[-\tau \frac{V(r_{i+1}) + V(r_i)}{2}\right], \tag{3}$$

where $\lambda^2 = \hbar^2\beta/m$, $2\pi\hbar$ being Planck's constant and m the particle mass. The first two factors in (3) represent the free particle part of the density matrix, while the third factor represents the effect of the potential field as a perturbation on the free particle. The thermal average of a quantity $A(r)$ is

$$\langle A \rangle = \left(\frac{P}{2\pi\lambda^2}\right)^{3P/2} \int \cdots \int \left\{ \prod_{i=1}^{P} dr_i \times \exp\left[-\frac{P}{2\lambda^2} \sum_{i=1}^{P} (r_{i+1} - r_i)^2 - \frac{\beta}{P} \sum_{i=1}^{P} V(r_i)\right] A(r_i) \right\}. \tag{4}$$

This can be formally related to a ring polymer in a field V and whose beads interact harmonically with their nearest neighbours with an elastic constant equal to $P/\lambda^2\beta$. Approximation (3) is exact when $P \to \infty$. In practice, P must be large enough for the potential energy to remain approximately constant within the length $\lambda_\tau = (\hbar^2\tau/m)^{1/2}$. For smooth potentials P can be of the order of 100. On the other hand, for hard-core potentials, P must be much larger. This creates two difficulties. First, the larger P is, the more rigid the corresponding polymer becomes and a conventional Metropolis sampling leads to very low acceptance ratios. Second, in the case of hard-core systems, the quantum particle may become trapped in one of the many potential minima, due to the barriers that separate them.

* Rutherford Appleton Lab, Chilton, Didcot, Oxfordshire OX11 0QX, U.K.

0021-9991/93 $5.00

These difficulties may be tackled either by (1) improving the expression of the propagator [2, 3] or (2) by devising new sampling schemes that speed up the equilibration, including the sampling of the normal modes of the polymer [4], the closely related Fourier series path integral technique [5–7], and the staging algorithm [3]. Here we follow the second strategy and derive two sampling schemes which are inspired by the staging algorithm [3]. The performance of the two schemes is compared with that of others for different systems.

2. MODIFIED STAGING ALGORITHMS

We follow Sprik *et al.* [3] and consider the ring polymer in two stages: in a first stage a so-called A-chain is defined with P_a beads r_i^a,

$$r_i^a \quad (i=0, ..., P_a) \qquad \text{with} \quad r_0^a \equiv r_{P_a}^a; \tag{5}$$

a second stage, the B-chain, is defined by inserting extra beads within those of the A-chain. That is, the B-chain beads have coordinates r_{ij}^b,

$$\begin{aligned} &r_{ij}^b \quad (i=1, ..., P_a; j=0, ..., P_b) \qquad \text{with} \quad r_{iP_b}^b \equiv r_i^a \\ &r_{ij}^b = R_{ij}^b + \Delta_{ij}, \qquad \text{with} \quad \Delta_{i0} = \Delta_{iP_b} = 0 \\ &R_{ij}^b = r_{i-1}^a + j(r_i^a - r_{i-1}^a)/P_b. \end{aligned} \tag{6}$$

It is seen from (6) that the B-chain beads are generated here as deviations from the straight line connecting two adjacent A-chain beads. Sprik *et al.* have shown that (4) can then be transformed to

$$\begin{aligned} \langle A \rangle = \left(\frac{P_a P_b}{2\pi\lambda^2}\right)^{3P_aP_b/2} \int \cdots \int \prod_{i=1}^{P_a} dr_i^a \prod_{i=1}^{P_a} \prod_{j=1}^{P_b-1} d\Delta_{ij} \\ \times \left\{ \exp\left[-\frac{P_a}{2\lambda^2} \sum_{i=1}^{P_a} (r_i^a - r_{i-1}^a)^2 \right. \right. \\ -\frac{P_a P_b}{2\lambda^2} \sum_{i=1}^{P_a} \sum_{j=1}^{P_b} (\Delta_{ij} - \Delta_{ij-1})^2 \\ \left. \left. -\frac{\beta}{P_a P_b} \sum_{i=1}^{P_a} \sum_{j=1}^{P_b} V(\{r_i^a\}, \{\Delta_{ij}\}) \right] A(r_i) \right\}. \end{aligned} \tag{7}$$

Both of the sampling schemes presented here are based on this expression and take the A-chain as a crude guide for the B-chain, as do Sprik *et al.* [3]. A major difference, however, is that the present procedures do not build the density matrix in stages; instead, they restrict staging to the sampling and always refer to the B-chain density matrix. A main advantage of concentrating on the B-chain is that the larger number of beads of this chain allows the use of the high-temperature approximation of the density matrix. A further difference is that here the acceptance criteria are defined as in Metropolis *et al.* [8].

2.1. *Modified Staging Algorithm I*

According to the condition of microscopic reversibility, the acceptance criterion for a move of $R \to R'$ is

$$A(R'/R) = \text{Min}\left[1, \frac{T(R/R')\,P(R')}{T(R'/R)\,P(R)}\right], \tag{8}$$

where $T(R'/R)$ is the transition probability from configuration R to R' and $P(R)$ is the equilibrium distribution, i.e.,

$$P(R) = \exp\left[-P_a T^a - P_a P_b T^\Delta - \frac{\beta}{P_a P_b} V \right], \tag{9}$$

where

$$T^a = \frac{1}{2\lambda^2} \sum_{i=1}^{P_a} (r_i^a - r_{i-1}^a)^2 \tag{10}$$

$$T^\Delta = \frac{1}{2\lambda^2} \sum_{i=1}^{P_a} \sum_{j=1}^{P_b} (\Delta_{ij} - \Delta_{ij-1})^2 \tag{11}$$

$$V = \sum_{i=1}^{P_a} \sum_{j=1}^{P_b} V(\{r_i^a\}, \{\Delta_{ij}\}). \tag{12}$$

In this algorithm, first an A-chain bead is moved. If this move is accepted, then the two sets of P_b beads in the B-chain connected with the A-chain bead are also generated. The moves of the B-chain beads are thus strongly correlated with the A-chain bead moves.

Let the beam moves be generated with a random uniform distribution in a box. In this case

$$\frac{T(r_i^a/r_i'^a)}{T(r_i'^a/r_i^a)} = 1 \tag{13}$$

and the acceptance criterion is

$$A_1(r_i'^a/r_i^a) = \text{Min}\left[1, \exp\left(-\frac{\beta}{P_a P_b} \Delta V_i^a - P_a \Delta T_i^a \right)\right] \tag{14}$$

with

$$\Delta V_i^a = \sum_{i=1}^{P_a} \sum_{j=1}^{P_b} (V(\cdots, r_i'^a, \cdots) - V(\cdots, r_i^a, \cdots)) \tag{15}$$

and

$$\Delta T_i^a = \frac{1}{2\lambda^2}\left[(r_i'^a - r_{i-1}^a)^2 + (r_{i+1}^a - r_i'^a)^2 - (r_i^a - r_{i-1}^a)^2 - (r_{i+1}^a - r_i^a)^2\right]. \tag{16}$$

To determine the acceptance criteria for the B-chain bead moves we must note that the latter only occurs if the A-chain move has been accepted. The probability of generating B-chain moves must contain this condition. Because of the form of (7), however, the generation of the values of the variables Δ_{ij} is independent of the values of the r_i^a coordinates and the transition probability for a B-chain move is the product of the transition probability for the Δ_{ij} change with the probability that the r_i^a move has been accepted. For the B-chain beads connected to r_i^a we obtain

$$\frac{T((\{r_{i+1j}^b\}, \{r_{ij}^b\})/(\{r_{i+1j}'^b\}, \{r_{ij}'^b\}))}{T((\{r_{i+1j}'^b\}, \{r_{ij}'^b\})/(\{r_{i+1j}^b\}, \{r_{ij}^b\}))} = \frac{\mathrm{Min}[1, \exp(+(\beta/P_aP_b)\,\Delta V_i^a + P_a\,\Delta T_i^a)]}{\mathrm{Min}[1, \exp(-(\beta/P_aP_b)\,\Delta V_i^a - P_a\,\Delta T_i^a)]} = \exp\left(+\frac{\beta}{P_aP_b}\Delta V_i^a + P_a\,\Delta T_i^a\right) \tag{17}$$

and the acceptance criterion is

$$A_{\mathrm{I}}((\{r_{i+1j}'^b\}, \{r_{ij}'^b\})/(\{r_{i+1j}^b\}, \{r_{ij}^b\})) = \mathrm{Min}\left[1, \exp\left(+\frac{\beta}{P_aP_b}(\Delta V_i^a - \Delta V_i^b) - P_aP_b\,\Delta T_i^{\Delta}\right)\right], \tag{18}$$

where

$$\Delta V_i^b = \sum_{j=1}^{P_b}\left(V(\cdots, \{\Delta_{i+1j}'^b\}, \{\Delta_{ij}'^b\}, \cdots) - V(\cdots, \{\Delta_{i+1j}^b\}, \{\Delta_{ij}^b\}, \cdots)\right) \tag{19}$$

and

$$\Delta T_i^{\Delta} = \frac{1}{2\lambda^2}\sum_{j=1}^{P_b}\left[(\Delta_{i+1j}' - \Delta_{i+1j-1}')^2 + (\Delta_{ij}' - \Delta_{ij-1}')^2 - (\Delta_{i+1j} - \Delta_{i+1j-1})^2 - (\Delta_{ij} - \Delta_{ij-1})^2\right]. \tag{20}$$

Using a random uniform distribution already induces diffusion of the quantum particle. The amount of diffusion may be further increased by periodic center-of-mass moves. These do not alter the configuration of the chain that represents the electron (thus keeping its kinetic energy constant), but they do change its potential energy. The corresponding acceptance criterion $A(\{r_{ij}'^b\}/\{r_{ij}^b\})_{\mathrm{cm}}$ is

$$A(\{r_{ij}'^b\}/\{r_{ij}^b\})_{\mathrm{cm}} = \mathrm{Min}\left[1, \exp\left(-\frac{\beta}{P_aP_b}(V(\{r_{ij}'^b\}) - V(\{r_{ij}^b\}))\right)\right]. \tag{21}$$

2.2. *Modified Staging Algorithm II*

The second modified staging algorithm breaks further away from that suggested in [3]. It relies on the fact, clearly indicated in expression (7), that the variables r_i^a and Δ_{ij} are independent. Here, when an A-chain bead r_i^a is moved, two sets of associated P_b beads are created, with the same deviations Δ_{ij}, but relative to the two new lines limited by r_{i-1}^a, $r_i'^a$ and $r_i'^a$, r_{i+1}^a, respectively. Expression (11) will remain unchanged and the acceptance criterion for this move is

$$A_{\mathrm{II}}(r_i'^a, \{r_{ij}'^b, r_{i+1j}'^b\}/r_i^a, \{r_{ij}^b, r_{i+1j}^b\}) = \mathrm{Min}\left[1, \exp\left(-P_a\,\Delta T_i^a - \frac{\beta}{P_aP_b}\Delta V_{\mathrm{II}}\right)\right] \tag{22}$$

where

$$\Delta V_{\mathrm{II}} = V(r_i'^a, \{r_{ij}'^b, r_{i+1j}'^b\}) - V(r_i^a, \{r_{ij}^b, r_{i+1j}^b\}). \tag{23}$$

The moves of the B-chain beads are generated by sampling the variables Δ_{ij} separately. The acceptance criterion for the latter is

$$A_{\mathrm{II}}(\Delta_{ij}'/\Delta_{ij}) = \mathrm{Min}\left[1, \exp\left(-P_a\,\Delta T_{\mathrm{II}}^{\Delta} - \frac{\beta}{P_aP_b}\Delta V_{\mathrm{II}}^{\Delta}\right)\right], \tag{24}$$

where

$$\Delta T_{\mathrm{II}}^{\Delta} = \frac{1}{2\lambda^2}\left[(\Delta_{ij}' - \Delta_{ij-1})^2 + (\Delta_{ij+1} - \Delta_{ij}')^2 - (\Delta_{ij} - \Delta_{ij-1})^2 - (\Delta_{ij+1} - \Delta_{ij})^2\right] \tag{25}$$

abd

$$\Delta V_{\mathrm{II}}^{\Delta} = V(\cdots, \Delta_{ij}', \cdots) - V(\cdots, \Delta_{ij}, \cdots). \tag{26}$$

As for Algorithm I, also in this case the center of mass moves may be attempted periodically, with the same acceptance criterion (21).

In both algorithms, the gaussian part of the acceptance criteria can be avoided using Levy's interpolation formula for a conditional Brownian motion to sample directly from the gaussian distribution [9, 10]. However, we have found that the acceptance criteria specified above are computationally more efficient.

Let us emphasize at this point the difference between the two modified staging algorithms just described and the original staging algorithm [3]. In the two algorithms proposed here, acceptance of the A-chain bead move does not involve the generation of a large number of the two associated B-chain portions that characterizes the original staging algorithm.

Let us also emphasize the difference between the two algorithms now proposed. Algorithm I follows the original staging algorithm closely in that r_i^a and r_{ij}^b are treated as the main variables. Algorithm II treats r_i^a and Δ_{ij} as the main variables. Thus, in Algorithm II, moving an A-chain bead drags the two connecting B-chain portions with it, but maintaining the values of Δ_{ij}, and each B-chain bead can be moved independently by sampling Δ_{ij} separately.

A resemblance between the two algorithms presented here and that of Pollock and Ceperley [2] is that both resort to multibead moves. A distinction is that already shared with the staging algorithm [3], namely that the latter allows bead moves in different length scales, large for the soft A-chain and smaller for the more rigid B-chain. As stated in [3], these different length scales are very important for overcoming the large barriers encountered in systems such as that described in Section 3.2. On the other hand, Pollock and Ceperley's method [2] relies essentially on improved expressions for the density matrix elements.

3. APPLICATIONS

Some controversy remains as to the best estimator for the kinetic energy of a quantum particle [11–14]. It has been pointed out that Barker's estimator [11] leads to a variance in the mean that increases linearly with the number of beads, P_aP_b [12]. On the other hand, Berne's estimator introduces a correlation with the potential energy which has a greater than linear growth with P_aP_b [13]. More recently, however, it has been shown that the latter considerations are in fact algorithm-dependent, the general conclusion being that Berne's estimator is to be preferred for algorithms involving multistep moves [14], such as the two described above. However, Berne's estimator cannot be used in the next two cases (for which the potential energy is either zero or infinity) and in this paper all the values of the kinetic energy have been evaluated using Barker's estimator:

$$E_K = \frac{3P_aP_b}{2\beta} - \frac{P_aP_b}{2\beta\lambda^2}\sum_{i=1}^{P_a}\sum_{j=1}^{P_b}(r_{ij}^b - r_{ij-1}^b)^2. \tag{27}$$

The potential energy E_P which is finite for an electron in helium is estimated as

$$E_P = \frac{1}{P_aP_b}\sum_{i=1}^{P_a}\sum_{j=1}^{P_b} V(r_{ij}^b). \tag{28}$$

A quantity that has been identified as a good indicator of the relative influence of the ground state and the excited states in the thermodynamic properties of an extra electron is the bead–bead mean square displacement $R^2(t-t')$ [15, 16]:

$$R^2 = \langle\langle |r(t) - r(t')|^2 \rangle\rangle, \tag{29}$$

t being the imaginary time and $\langle\langle \cdots \rangle\rangle$ indicating thermal averaging. For a free electron, R^2 is parabolic, while for a localized electron a *plateau* appears, due to the strong influence of the ground state. $R(\beta\hbar/2)$ can be taken as a measure of the electron size.

A pass is defined as a set of Monte Carlo moves in which all the particles have been moved once. The number of electron passes for Algorithm I is calculated as

$$N_{\text{pass}}^{\text{I}} = (N^a + N^\Delta * 2 * (P_b - 1))/P_aP_b, \tag{30}$$

where $N^{a(\Delta)}$ is the number of A (B)-chain bead moves attempted. For Algorithm II we have, instead,

$$N_{\text{pass}}^{\text{II}} = (N^a * (2P_b - 1) + N^\Delta)/P_aP_b. \tag{31}$$

The number of accepted passes $N_{\text{pass}}^{\text{acc}}$ can be obtained by substituting $N^{a(\Delta)}$ by $N_{\text{acc}}^{a(\Delta)}$, the number of A (B)-chain bead moves accepted. There are no established rules as to what is the optimal acceptance ratio $N_{\text{pass}}^{\text{acc}}/N_{\text{pass}}$ in a Monte Carlo simulation [17]. Our simulations indicated that the value of the acceptance ratio is more important for Algorithm I, for which a value larger than 50% leads to a rapid convergence of the structural properties such as the size, while a value lower than 10% was found best for the convergence of the kinetic energy. In both cases performances are optimized by keeping the acceptance ratio for A-chain bead moves smaller than that of the B-chain.

The simulations were made on the University of London Computer Centre Cray X-MP/28 and on the Cray X-MP/416 at RAL and the computational time will be specified in each case. The errors indicated correspond to the standard error corrected by the inefficiency of the sampling as estimated in [13].

3.1. *The Free Electron*

Because (3) is an exact solution of the quantum-free particle, valid for any number of beads, this very simple system constitutes the most direct and simple way of checking the

computer programs and of making a preliminary test of the performance of the two algorithms. Table I gives the results of simulations for three different values of P_a and P_b. In each row the top line is for Algorithm I and the bottom line is for Algorithm II. When more than one CPU time is displayed for a specific number of beads, the shorter times are intermediate results to demonstrate the convergence of that simulation. Table I shows that, as far as the electron size is concerned, both algorithms converge equally fast (the standard errors for size are smaller than 0.1% in all cases and are not indicated). The same does not apply to the kinetic energy which indicates that Algorithm II performs better than I. This is true even for a small number of beads, as is clearly seen from the respective standard errors. The better performance of Algorithm II is due to its being more effective in sampling configuration space, which is related to the lack of correlation between the A-chain bead and the B-chain bead moves. Furthermore, it generates a greater number of passes per CPU second.

TABLE I

The Free Particle (Atomic Units)

P_a	P_b	βE_K	Size	Passes	CPU(s)
4	4	1.52 ± 0.09	5.01	514390	100
		1.49 ± 0.03	4.99	932250	
8	8	1.49 ± 0.50	4.99	571370	300
		1.42 ± 0.09	5.00	823680	
		1.42 ± 0.31	4.98	1175425	600
		1.53 ± 0.08	4.98	1659190	
16	8	1.82 ± 1.30	5.00	456523	600
		1.35 ± 0.13	4.99	726000	
		1.73 ± 0.28	4.98	1132810	1500
		1.42 ± 0.09	4.99	1789920	
∞	∞	1.50	5.0		

In a more complete assessment of the two algorithms it is important to determine whether these results are system dependent. The systems chosen are interesting from the latter and also from a purely physical point of view. Indeed, the steepness of the potential field makes the electron in a hard spheres system one of the most difficult to model by path integral Monte Carlo. On the other hand, from the physical point of view, hard core interactions constitute one of the essential ingredients of the interaction of an electron with any atom. The excess electron in a liquid helium system has a finite potential and has also been well studied experimentally [18].

3.2. *An Electron in a Hard Spheres Crystal*

The potential for the interaction of an electron with a hard sphere is

$$\begin{aligned} &V(\{r_{ij}^b\}) = 0 \quad \bigvee_{ijs} |r_{ij}^b - r_s^h| > \sigma/2 \\ &V(\{r_{ij}^b\}) = \infty \quad \ni_{ijs} |r_{ij}^b - r_s^h| \leqslant \sigma/2 \\ &(i = 1, ..., P_a; j = 1, ..., P_b; s = 1, ..., M); \end{aligned} \tag{32}$$

σ is the diameter of the hard spheres and r_s^h, $s = 1, ..., M$, represents the coordinates of the M hard spheres. In our simulations M was 432.

We have considered a temperature such that $\lambda = 6\sigma$, a density $\rho\sigma^3 = 0.201$, ρ being the number density of the hard sphere system and a minimum distance d of approach between the electron and the hard spheres of $d/\sigma = 0.5$. These values define a whole class of situations parametrized by the actual value of σ. Table II displays the results obtained. The exact value quoted for the kinetic energy is calculated by combining the Wigner–Seitz and pseudopotential methods [19]. As expected, the number of beads needed to obtain convergence in this system is much larger. This can, of course, be improved by the use of higher order approximations for the propagator (1). As an empirical rule we found that the larger the size of the electron, the greater the number of beads needed for an accurate representation. Therefore, the extended states of electrons in a crystal, such as those in Table II constitute some of the hardest to simulate.

Table II shows that the faster convergence of the kinetic energy for Algorithm II already observed, is here much more marked. One of the causes is the also very marked decrease in the number of passes (compared to those achieved by Algorithm II in the same CPU time). This is because the generation of two B-chains becomes more and

TABLE II

Electron in a Hard Spheres Crystal (Atomic Units)

P_a	P_b	βE_K	Size	Passes	CPU(s)
128	32	214 ± 22	4.60 ± 0.01	8169	10000
		54 ± 5	3.73 ± 0.39	41712	
		231 ± 23	4.52 ± 0.01	11959	15000
		58 ± 5	4.26 ± 0.69	61834	
					20000
		55 ± 5	4.56 ± 0.77	81515	
128	64	1271 ± 111	4.82 ± 0.04	6637	15000
		67 ± 7	4.19 ± 0.21	35001	
		1204 ± 121	4.86 ± 0.04	8741	20000
		73 ± 8	4.53 ± 0.38	45956	
		1153 ± 125	4.93 ± 0.05	10796	25000
		71 ± 7	4.71 ± 0.40	56643	
∞	∞	74	4.8?[a]		

[a] Estimated from the simulation.

more time consuming as P_b increases. This is overcome by letting the A-chain acceptance ratio decrease. However, as Table II indicates, the convergence ratio of the kinetic energy is still much worse than that of Algorithm II. On the other hand, a reverse behaviour is observed for the structural properties such as the size. This is already apparent in Table II and becomes enhanced if the acceptance ratios for Algorithm I are increased (results not shown). However, the convergence rate of structural properties for Algorithm II is only about 0.5–0.75 that of Algorithm I and therefore does not compare with the slowness of the convergence rate for the kinetic energy of Algorithm I.

The results shown in Table II are for a relatively low density of $\rho\sigma^3 = 0.201$. As the density increases, it becomes more difficult to overcome the infinite barriers that the hard spheres represent. Simulations with $\rho\sigma^3 = 0.5$ showed, however, that the rates of convergence of the two algorithms proposed here are essentially those indicated in Table II.

In summary, our simulations indicate that for this system there is a specialization, and while the kinetic energy is best calculated with Algorithm II, the investigation of structural properties such as the size and those presented in Section 3.4 is better made with Algorithm I.

3.3. *An Electron in Helium*

The electron–helium interaction is modelled using the pseudopotential as parametrized by Coker *et al.* [20], while the helium–helium interaction is a standard Lennard–Jones potential with $\sigma_{He}^{LJ} = 2.556$ Å and $\varepsilon_{He} = 10.22$ K [20].

Table III shows the results of simulations with $T = 309$ K and $\rho\sigma_{He}^{LJ}\ 3 = 0.5$. It is readily apparent that the number of beads needed for a good representation of the quantum properties of the electron in helium is much smaller than that needed for an electron in a hard spheres crystal. $P < 1000$ is the expected requirement for a smooth potential.

It is the standard interpretation that electrons in helium are trapped in bubbles [18, 20]. Our results are in agreement with those of Coker *et al.* [20] and corroborate that interpretation. In fact, the values of the kinetic energy in our simulations are even closer to that of an electron in a spherical box [20]. Slight discrepancies between our and Coker *et al.*'s results may be due to the fact that while the latter introduced a cutoff of $2.5\sigma_{He}^{LJ}$, we have considered interactions between all particles in the system.

Also here we notice the specialization that is manifest for the hard sphere system, with Algorithm I performing better for the structural properties, including the potential energy. The differences are nevertheless not so dramatic in the case of Algorithm II which comes out as a more balanced and more efficient algorithm for this smoother potential.

3.4. *A Hard Sphere Model of an Electron in Helium*

Since the electron–helium potential used in the last subsection is essentially repulsive it is interesting to find out whether a hard sphere model, with suitably defined parameters, is able to reproduce the properties of an electron in helium. A similar study has been made before [21], but a different fitting procedure led to a different hard sphere system. For the hard sphere system, σ is well defined as the shortest distance that two particels can approach each other, which can be retrieved from the respective radial distribution function (RDF) which exhibits a discontinuity at that value. Because of the continuous nature of the Lennard–Jones potential, however, the corresponding RDF also varies continuously, which makes the definition of distance of minimum approach rather ambiguous. Here, an effective σ is defined so that a best comparison between the

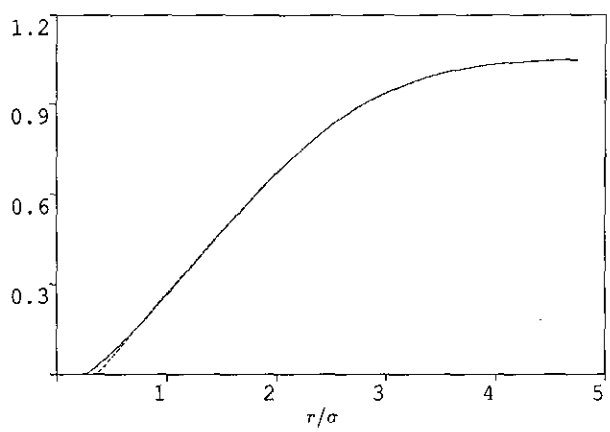

FIG. 1. The electron bead–solvent radial distribution function $g(r)$ for an electron in helium (solid line) and a hard spheres fluid (dashed line) (see text).

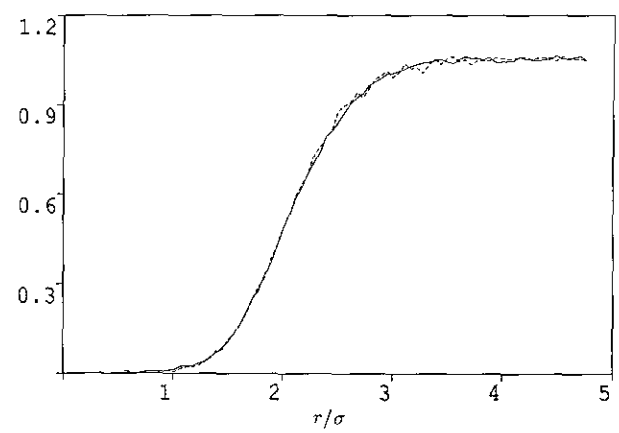

FIG. 2. The electron center of mass–solvent radial distribution function $g_{cm}(r)$ in helium (solid line) and a hard spheres fluid (dashed line) (see text).

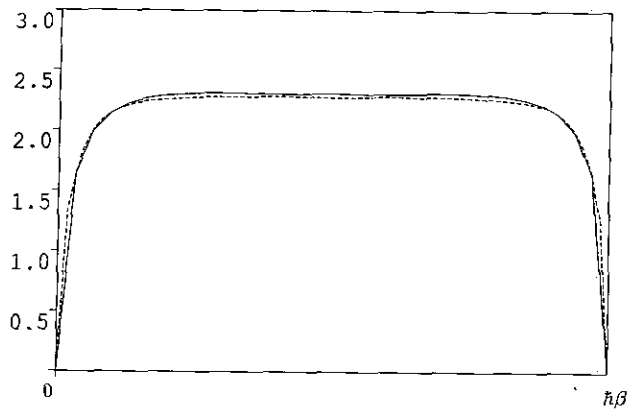

FIG. 3. The electron bead–electron bead mean square displacement R in helium (solid line) and a hard spheres fluid (dashed line) (see text).

two systems is obtained. Figures 1–4 show the results for a hard sphere fluid with $\rho\sigma^3 = 0.035$, $\lambda/\sigma = 16$, and $d/\sigma = 1.2$. Figures 1–3 show that the behaviour of the electron is indeed well represented by this hard sphere model. In particular, the "bubble" associated with the electron in helium is also observed for the electron in this hard spheres fluid, as is clearly seen from Figs. 1 and 2 which show the RDFs; i.e., the distance of closest approach of the electron center of mass to the hard spheres is about three times that of the individual electron beads to the hard spheres. This means that the electron is enclosed by, rather than wrapping around, the hard spheres, forming a bubble. The structural similarity displayed in Figs. 1–4 is also apparent in the kinetic energy which in this model is 35 ± 6, a value that compares well with those in Table III.

These results show that bubble formation for an electron in helium is due to excluded volume effects. This same conclusion was reached by previous studies [20, 21]. However, the equivalent hard sphere system in Laria and Chandler's article [21] is different from ours. This is due to the difference in the fitting procedure: while ours is made in real

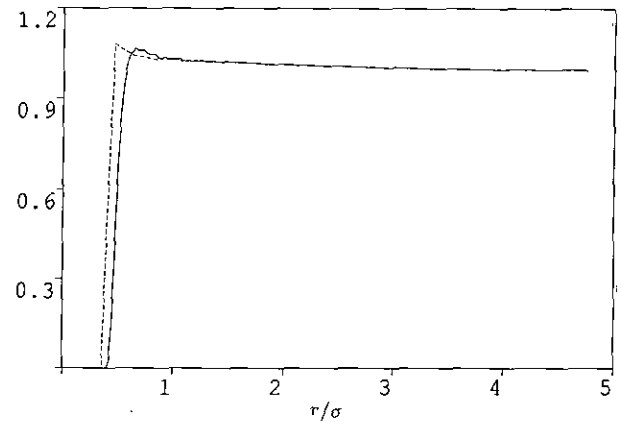

FIG. 4. The solvent–solvent radial distribution function $g_{hh}(r)$ in helium (solid line) and a hard spheres fluid (dashed line) (see text).

TABLE III

Electron in Liquid Helium (Atomic Units)

P_a	P_b	βE_K	βE_P	Size	Passes	CPU(s)
16	16	11 ± 3	4.77 ± 0.18	2.28 ± 0.02	15912	3700
		24 ± 1	5.60 ± 0.14	2.33 ± 0.02	20613	
		17 ± 5	4.93 ± 0.12	2.29 ± 0.01	31563	6700
		23 ± 1	5.66 ± 0.09	2.36 ± 0.01	41227	
32	16	27 ± 10	5.22 ± 0.07	2.30 ± 0.01	14435	6000
		25 ± 2	5.13 ± 0.18	2.29 ± 0.03	18371	
		30 ± 10	5.14 ± 0.06	2.30 ± 0.01	21478	8000
		24 ± 2	5.19 ± 0.18	2.28 ± 0.02	27542	
		26 ± 9	5.26 ± 0.09	2.31 ± 0.01	28375	10000
		25 ± 1	5.13 ± 0.11	2.27 ± 0.02	36685	
*		$27 \pm ?$	6.5 ± 1	$2.2 \pm ?$		14400

* $P \approx 1000$, from Ref. [15].

space, Laria and Chandler's is made in k-space. They evaluate the structure factor of the helium system and determine the hard sphere diameter and density such that its structure factor's first peak position and height coincide with that of the helium system. This leads to a larger σ and a correspondingly larger density than we report here. Our main aim is to obtain a good representation for the electron, while Laria and Chandler's fitting procedure concentrates on the helium system. The success of our fitting procedure as far as the electron states are concerned can be judged from Figs. 1–3. On the other hand, the approximation involved in the representation of the helium system by the hard sphere system we have selected can be measured from the difference of the respective RDFs shown in Fig. 4.

4. DISCUSSION AND CONCLUSION

We propose two sampling schemes for path integral Monte Carlo simulations which bring together a staging procedure and conventional Metropolis sampling. In Algorithm I there is a dependence between the moves of the two stages, while in Algorithm II the two stages move in an independent way. They are highly vectorisable and thus particularly suited for supercomputers and, also, they are flexible and not machine directed, unlike the original staging algorithm of Sprik *et al.* [3] which was tailored to the Cyber 205.

We have tested the performance of the two sampling schemes in different systems. While the free electron can be regarded as an exercise to check the algorithms and make a preliminary probe of their performance, the hard sphere model and the helium model are interested from more than one point of view. Indeed, from a computational point of view, path integral simulations are more difficult the steeper

the potential field is and thus the hard sphere model provides a stringent test for the performance of an algorithm. From the physical point of view, the hard sphere model is a basic model for electron solvation [15, 16]. The helium model, on the other hand, provides a test of the performance of the algorithms for smoother potentials and physically is a system on which a great wealth of information has been accumulated [18]. Both algorithms perform very well as far as the structural properties are concerned and the CPU time involved is competitive with other algorithms. Most striking is the convergence of the kinetic energy of the electron for Algorithm II. Indeed, the kinetic energy is one of the slowest quantities to converge and its estimation in previous studies of the electron in a hard sphere system involved resorting to a higher approximation of the density matrix [3]. Here we employ only the primitive algorithm (3) and obtain the kinetic energy of the electron in shorter CPU times. The same applies to the simulation of the electron in helium, for which the kinetic and potential energies and the electron size converge in less than half the time of other methods [20]. In short, the flexibility demonstrated by the algorithms in dealing with both steep and smooth potentials, as well as their efficiency and machine adaptability make them (especially Algorithm II) generally very useful for path integral calculations.

We have also confirmed that the properties of an electron in helium can be simulated with a hard sphere fluid model. Here, the bubble formation, which in other systems is due to an *attractive* interaction between the electron and the solvent, is caused by a strong *repulsion* between the electron and the solvent. This is in agreement with a previous study by Laria and Chandler that showed that the behaviour of an electron in helium can be understood essentially in terms of excluded volume effects. The hard sphere equivalent model presented here is, however, different from that of Laria and Chandler because of the difference in fitting procedures.

ACKNOWLEDGMENTS

This work is supported by the U.K. Science and Engineering Research Council and the Medical Research Council.

REFERENCES

1. R. P. Feynman, *Statistical Mechanics* (Benjamin, Reading, MA, 1972).
2. E. L. Pollock and D. M. Ceperley, *Phys. Rev. B* **30**, 2555 (1984).
3. M. Sprik, M. L. Klein, and D. Chandler, *Phys. Rev. B* **31**, 4234 (1985).
4. J. Bartholomew, R. Hall, and B. J. Berne, *Phys. Rev. B* **32**, 548 (1985).
5. J. D. Doll and D. L. Freeman, *J. Chem. Phys.* **80**, 2239 (1984).
6. J. D. Doll, R. D. Coalson, and D. L. Freeman, *Phys. Rev. Lett.* **55**, 1 (1985).
7. R. D. Coalson, *J. Chem. Phys.* **85**, 926 (1986).
8. N. Metropolis, A. W. Rosenbluth, M. N. Rosenbluth, A. H. Teller, and E. Teller, *J. Chem. Phys.* **21**, 1087 (1953).
9. P. Levy, *Mem. Sci. Math. Fasc.* Vol. 126 (Gauthier–Villars, Paris, 1954).
10. L. D. Fosdick and H. F. Jordan, *Phys. Rev.* **143**, 58 (1966).
11. J. Barker, *J. Chem. Phys.* **70**, 2914 (1979).
12. M. F. Herman, E. J. Bruskin, and B. J. Berne, *J. Chem. Phys.* **76**, 5150 (1982).
13. A. Giansanti and G. J. Jacucci, *J. Chem. Phys.* **89**, 7454 (1988).
14. J. Cao and B. J. Berne, *J. Chem. Phys.* **91**, 6359 (1989).
15. D. Chandler, Y. Singh, and D. M. Richardson, *J. Chem. Phys.* **81**, 1975 (1984).
16. A. L. Nichols III, D. Chandler, Y. Singh, and D. M. Richardson, *J. Chem. Phys.* **81**, 5109 (1984).
17. M. P. Allen and D. J. Tildesley, *Computer Simulations of Liquids* (Clarendon Press, Oxford, 1987), p. 122.
18. See H. T. Davis and R. G. Brown, *Adv. Chem. Phys.* **31**, 329 (1975) and references therein.
19. B. E. Springett, J. Jortner, and M. H. Cohen, *J. Chem. Phys.* **48**, 2720 (1968).
20. D. F. Coker, B. J. Berne, and D. J. Thirumalai, *J. Chem. Phys.* **86**, 5689 (1987).
21. D. Laria and D. J. Chandler, *J. Chem. Phys.* **87**, 4088 (1987).